Wear 270 (2011) 479–491

Contents lists available at ScienceDirect

Wear

journal homepage: www.elsevier.com/locate/wear

Correlation between laboratory ball-on-disk and full-scale rail performance tests

Francisco C. Robles Hernández[a,b,*,1], Nicholaos. G. Demas[c], Kari Gonzales[a], Andreas A. Polycarpou[c]

[a] Transportation Technology Center Inc. (TTCI), 55500 DOT Rd., Pueblo, CO 81001, USA
[b] University of Houston, College of Technology, Mechanical Engineering Technology, 304 Technology Building, Houston, TX 77204-4020, USA
[c] Department of Mechanical Science and Engineering, University of Illinois at Urbana-Champaign (UIUC), Urbana, IL 61801, USA

ARTICLE INFO

Article history:
Received 24 June 2008
Received in revised form
23 December 2010
Accepted 5 January 2011
Available online 12 January 2011

Keywords:
Rail
Wheel-rail contact
Wear
Ball-on-disk
Workhardening
Sliding contact fatigue

ABSTRACT

Railroads in the United States spend approximately $2.5 billion a year on rail replacement and repairs, making rail the most valuable asset for the railroad industry in North America. The Transportation Technology Centre, Inc. (TTCI) continuously conducts full-scale rail performance tests using the newest generations of premium rails. This in turn allows better understanding of the rail characteristics that require improvements and is used to extend rail's life. Recent research has focused on methods to streamline the developments of prototype rail steels using laboratory tribotests. The results of the tribotests indicate that sliding ball-on-disk experiments can be used to qualitatively approximate rail wear and using scanning electron microscopy (SEM) it is possible to observe different tribological behaviour between rails (mild to severe wear). For instance, SEM micrograph analysis can lead to the determination of the propensity of rail crack formation under pure sliding and the detrimental effects of pro-eutectoid cementite and hard inclusions (e.g., Al_2O_3) on crack formation and delamination.

Published by Elsevier B.V.

1. Introduction

A major goal in the development of new rail materials is improving wear performance and rolling contact fatigue (RCF) through higher hardness [37,38]. Over time, a relationship between hardness and wear of rail steels has been observed [1]. Nonetheless, the initial (as manufactured) hardness of premium rails does not have a direct correlation with wear performance making the prediction of wear based on initial rail hardness difficult, in agreement with earlier works [2]. Increasing hardness is relatively easy to achieve by adding alloying elements to steel (mainly carbon) and applying heat treatments. However, there is a theoretical limit to the hardness that can be achieved in pearlitic steels [3–9] and current rail steels are approaching this limit.

Premium rails, previously known as high strength rails (HSR), are made out of high carbon steels with a pearlitic microstructure, and are mainly used for curves and tracks with high traffic in heavy axle load applications. The typical running surface for HSR has an approximate Brinell Hardness of 370 HB. Premium rails are characterized for their higher hardness, which results in better wear performance and fatigue resistant characteristics [1]. Bainite is an alternate microstructure that has been used for rails in the past and it can be harder than pearlite. Studies thus far have indicated that for rails, the pearlitic microstructure is more suitable than the bainitic microstructure particularly for the heavy haul service in North America [10,39]. Apparently, the success of pearlite over bainite is due to its better workhardening ability. Currently, new steel developments focus in the reduction, and ideally elimination, of inclusions and pro-eutectoid cementite along the prio-austenite grain boundary. Inclusions form during steel manufacturing and its amount can be reduced by using alternative technologies. The amounts of pro-eutectoid cementite can be controlled by reducing the amount of carbon and by advanced thermomechanical processing [11,29].

TTCI is wholly owned subsidiary of the Association of American Railroads, located in Pueblo, Colorado and continuously conducts full-scale rail performance tests at the Facility for Accelerated Service Testing (FAST). Previously, it was difficult to determine wear performance for individual rails using laboratory ball-on-disk method and correlate with full scale tests at FAST [1]. This was in-part due to the fact that at FAST the wear results were reported as total area loss while in ball-on-disk tests the results were reported based on the depth of the wear track. In this article, a more sophisticated approach involving the calculation of the total area loss is proposed. The area lost is directly compared to the FAST results. The improved analysis approach considers the wear volume inside the wear track including the total area of the metal flow on each side

* Corresponding author at: University of Houston, Mechanical Engineering Technology, 304 Technology Building, Houston, Tx 77204-4020, USA.
Tel.: +1 713 743 8231; fax: +1 505 213 7106.
E-mail address: fcrobles@uh.edu (F.C. Robles Hernández).
[1] Formerly at TTCI, Currently at the University of Houston.

0043-1648/$ – see front matter. Published by Elsevier B.V.
doi:10.1016/j.wear.2011.01.001

of the wear track (track shoulders) similar to the profile overlay method used at FAST.

2. Experimental procedure

FAST is a 4.4 km (2.73 mile) loop track. The train (or consist) at FAST has 80 cars and 4 locomotives, and each is loaded with 143 t. The rails at FAST are subjected to a nominal load of 35.5 t per axle. The train at FAST completes an average of 100 laps per day, equivalent to 440 km (273 miles), which corresponds to an accumulated load of 0.91 million gross metric tons MGMT (megatons) or 1 million gross tons (MGT) per day (*Note*: 1 MGMT = 1.1 MGT).

In this work we present the results of two generations of premium rails. The first is identified as "previous" generation (designated as "OLD") was manufactured in 2001 and tested at FAST from 2001 to 2005 after accumulating 435 MGMT (478 MGT). The second generation of rail is designated as "current" generation, was manufactured in 2005 and tested at FAST from 2005 to 2009 after accumulating 450 MGMT (495 MGT). In the present article we used the results of the current tests as of January 2008 after an accumulated traffic of 318 MGMT (350 MGT). Note also that there are five types of premium rails in the current generation and the results of the previous generation are used in this work for comparison purposes. The rails used for both tests were manufactured by several companies and are referred as: JFE Steel America Inc., Mittal, Nippon Steel Corporation, Corus, Rocky Mountains Steel Mills, and Voestalpine.

2.1. Full scale FAST tests

FAST is divided into 41 test sections, where different railroad track components are subjected to heavy haul environments. This allows accelerated degradation of testing components to have rapid performance identification. A section at FAST, identified as Section 7, is dedicated to premium rail evaluation. The section is a non-lubricated 5° curve that accelerates wear and exposes the rails to aggressive environmental conditions. Section 7 is 305 m (1000 ft) long with 10.2 cm (4 in.) super elevation and 4.3 cm (1.7 in.) cant deficiency. The 80 cars FAST train is operated at an average speed of 64.4 km/h (40 m/h) for 8 h every night to accumulate 1 MGT/night. Super elevation is the difference in height between low and high rails (low rail denotes the inner rail and high rail the outer rail in a curved track with curvature of 5°). Cant deficiency is the difference between the equilibrium elevation and the actual rail elevation. In the United States, a degree of curvature is defined as the central angle subtended by a chord of 30.48 m (100 ft). It means that one degree of curvature has a distance of 30.48 cm (1 ft) at the centre between the curve and the chord.

Fig. 1 indicates the direction in which the profile measurements were taken. The series of ascending numbers in parentheses identify each profile measurement location (note that 4 measurements per location were performed). The control rail is identified as rail B. The control rail was manufactured in 2005 and all rail sections were located on either end of every two test rail sections. All rails were flash butt-welded. Two profile measurements were taken on each test rail and the control rail at 120 and 240 cm (47 and 95 in.) from each weld.

Each rail manufacturer (except for the control rail) contributed with six 24.4 m (40 ft) rail sections for the FAST tests. Three of these sections were installed in the high rail and three in the low rail. Two sections of each rail were installed one on each end of the curve and the third section in the centre of the curve; similar distribution was made for the low and high rails, respectively. This rail distribution takes into account any potential effect of location along the curve and the rail wear results reported in this work are the average for each rail. The control rail has seven sections on each low rail and high rail. The larger number of control rail sections facilitated the rail performance analysis and were used to discriminate and identify any effects of location along the curve.

Brinell Hardness (HB) measurements were performed on the head of the rails at depths of 0.8 ± 0.2 mm (0.03 ± 0.001 in.) on the ground surface as specified by the American Railway Engineering and Maintenance-of-Way Association (AREMA) [12]. This practice is followed so that the hardness measurement is always taken below the decarburized layer.

Profile measurements at FAST were taken at 0 MGMT (control measurement) followed by measurements every 15 MGT through 105 MGT, then every 25 MGT until the end of the tests. The rail profiles are collected using a MiniProf® profile measurement tool and the data is analyzed using the associated MiniProf® software. The software is used to superimpose the profiles at the different tonnages and measure the precise area loss (wear). The profile measurement locations were fixed to ensure that the profiles were taken at the same location during every measurement. Before each measurement cycle, the rail surface is prepared by removing any impurities (including carryover grease) that can alter the profile measurements.

The measured profiles determine the wear, based on the diagonals W1, W2, or W3, as shown schematically in Fig. 2a. In this work, the analysis of rail wear is by area loss and Fig. 2b shows a typical cross section of a high rail's head removed from Section 7 after 396 MGT (435 MGMT), and Fig. 2c depicts an example of overlaid rail profiles showing how the rail profile is changing to determine the diagonals and the total area loss as a function of accumulated tonnage. Four measurements per rail section, as shown in Fig. 1 were taken at each of the above listed intervals, and average values are reported.

2.2. Laboratory ball-on-disk tribological tests

Tribological tests on the rail samples were conducted using a conventional ball-on-disk tribometre. The tribometre is a specialized pin-on-disk apparatus which can measure in situ friction and normal load data. It consists of a rotating/oscillating lower spindle on which the flat specimen is rigidly mounted, and a special top holder which applies a normal load in a controlled closed loop manner via an electromagnet. The ball specimen is mounted in a tubular collet assembly which is held stationary in a two axis water-cooled force transducer. The friction force, F, and the normal force, N, are measured in situ and the friction coefficient is directly calculated. The loading mechanism is an electromagnetic actuator which applies a normal load from zero to 22 N.

The experiments were performed under laboratory conditions of 22 °C and 40% RH. For the ball-on-disk tests, the wear data was collected after 50, 100, 300, 600, and 1000 cycles. A constant normal force of 10 N that corresponds to an initial Hertzian mean contact pressure of 2.5 GPa was applied for all tests [3]. This contact pressure is equivalent to the one observed on the rail gage faces of the high rail in Section 7 (Fig. 2, W2 and W3). On the rail head, the expected contact pressure is slightly lower (i.e., less than 2 GPa). The tests were performed at 100 revolutions per minute, which for the geometry used in this work corresponds to a linear speed of 0.06 m/s (thus each cycle corresponds to 6×10^{-4} m sliding distance). Following the tribotests, 4 mm wear scans were measured using a P-15 Tencor® contact profilometre, equipped with a 2.5 μm stylus radius. A 25 mg normal load was used for the measurements. The wear tracks produced during each tribotest were measured at four locations 90° from each other. The samples were named as rails A to E and as OLD.

Fig. 3 shows a general overview of the ball-on-disk test sample preparation procedure. The balls used for the tribotests are small

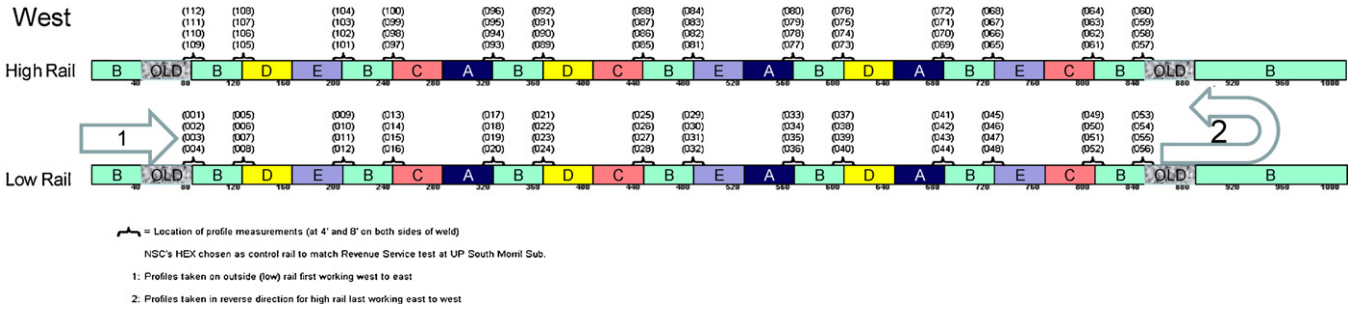

Fig. 1. Layout of FAST Section 7 rail steel evaluation. The length of the rail steel evaluation (Section 7) at FAST is 305 m and each section of rail measure is 24.3 m, 5° curve with 10.2 cm of super elevation and 4.3 cm of cant deficiency. Numbers in parentheses from 001 to 112 indicate the location where the wear measurements were conducted on the various rails. The Numbers 40–320 are the tie numbers. Rail labelled as "OLD" corresponds to the rail tested on the previous generation of rail testing.

synthetic ruby balls with a diameter of 1.6 mm (0.06 in.) and hardness of 1570–1800 Vickers. A new ruby ball and a rail steel disk were used for each test. This type of ruby ball is up to 4 times harder than the rail tested, so it was able to wear the rails without incurring wear. All disk samples were extracted 8 mm (0.32 in.) from the rail surface to eliminate the decarburized layer and extract the samples from comparable locations. The ball-on-disk samples were extracted using electrical discharge machining and ground to a finishing surface of a root-mean-square surface roughness of $R_q = 0.8\ \mu m$. Both the ruby balls and the samples were cleaned ultrasonically using acetone, followed by a rinse with 2-propanol, and dried with warm air before each test.

After the completion of the tribotests, the disks were again cleaned and the wear tracks were measured using profilometry. Some rails produced large amounts of debris during the wear tests and the debris was collected and deposited on graphite tape. Both the debris and the ball-on-disk test samples were analyzed using a Jeol-JSM-6060LV scanning electron microscope operated at 20 kV. The semi-quantitative chemical analysis was carried out using an electron dispersed X-ray (EDX) probe. The wear tracks on the samples were characterized directly after the tests to preserve the tribo-characteristics on the disk samples.

3. Results and discussion

3.1. Hardness tests

Table 1 compares the results of the initial hardness of the rails (designated as Used 1–6), which were obtained from rails manufactured in 2001 before and after full scale, FAST, testing. The initial head hardness of the rails manufactured in 2005 (designated as rails A–E) is also given in Table 1. The average rail head hardness for rails A through E in as-rolled conditions is 410 ± 23 HB. Table 1 illustrates that rails Used 1 through Used 6 have an initial hardness varying from 382 to 405 HB. After work hardening, the rails identified as Used 2, 4, and 6 showed similar increases in hardness, to 415 HB, while the hardness of rails designated as Used 3 and 5 increased to 429 HB and rail Used 1 to 461 HB. The above hardness changes raised the interest to conduct a multi-scale hardness analysis to better understand the rail work hardening phenomena.

The multi-scale hardness tests were conducted by means of nano-hardness, micro-Vickers hardness and Rockwell C hardness on FAST tested rails after 435 MGMT at depths between 30 μm and 100 μm. The hardness for the parent rail was measured from further away where no plastic deformation is observed. The results

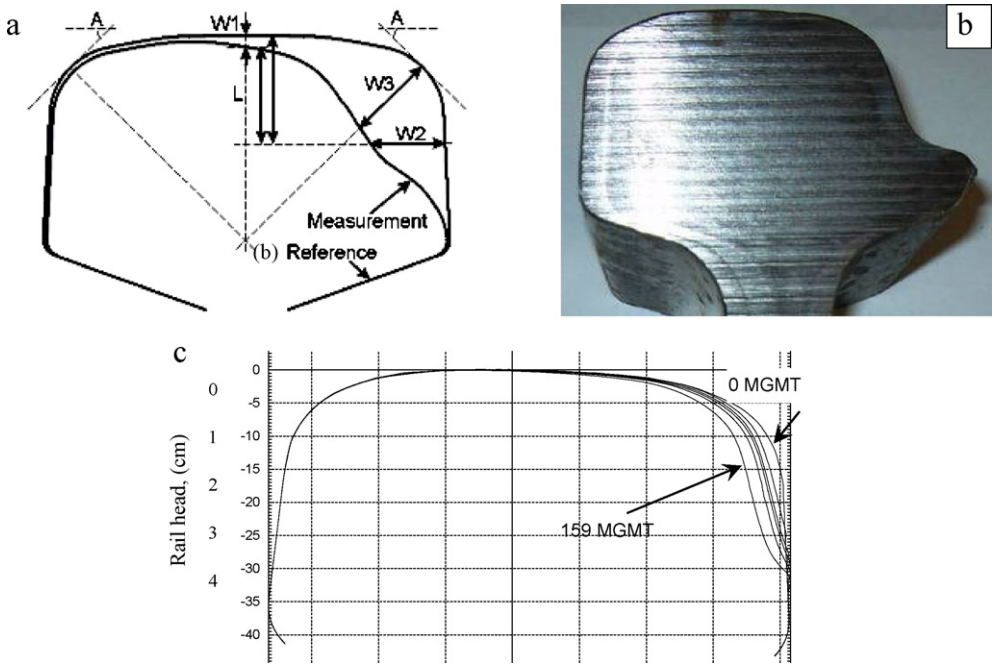

Fig. 2. (a) Sketch of rail head wear measurements, (b) photograph of a typical worn rail removed from FAST after 435 MGMT and (c) typical overlaid rail head profiles taken from 0 to 159 MGMT.

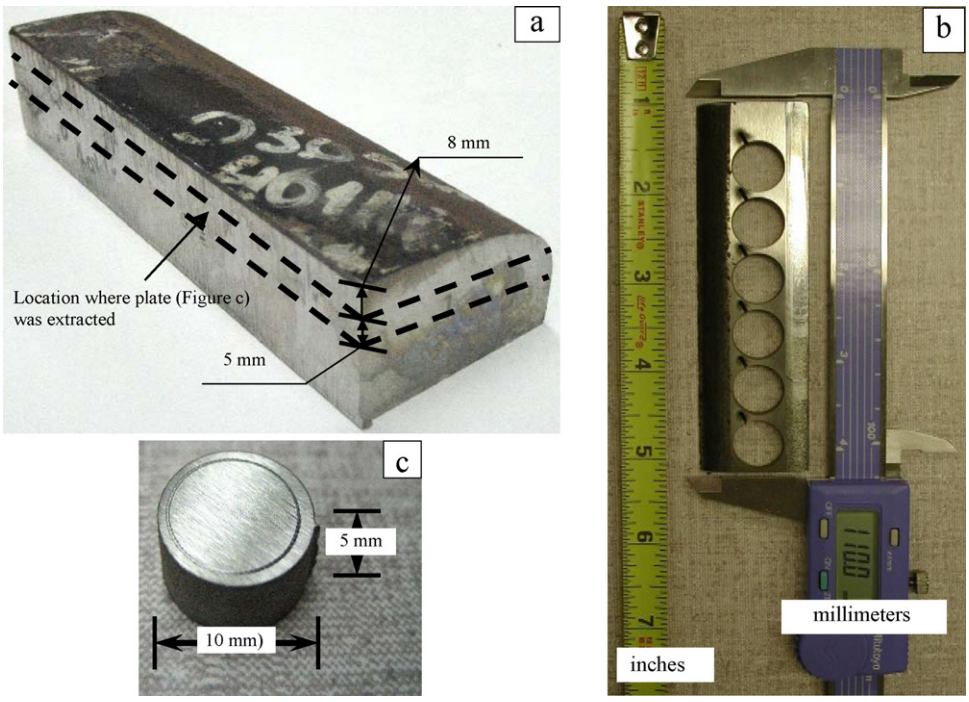

Fig. 3. Typical photographs of rail heads and extracted samples subjected to tribotesting: (a) half rail's head showing the location where the (b) steel plate was removed (dotted lines), and (c) tested disk showing a 300 cycles wear track.

of Vickers micro-hardness are approximately 420 HV for the parent rail and 746 HV for the near-surface hardness. This represents an increase of approximate 80%. Using nanohardness measurements, the values are as high as 1300 HV, which is about 300% increase; unfortunately, there is significant scatter in the nanohardness results, possibly due to the small size of the indenter with respect to the size of the Fe-α and Fe_3C lamellas that have markedly different hardness [13]. In the literature [17], it has been reported that Vickers microhardness values for Fe_3C (cementite) can be as high as 1250 HV, which is in agreement with the nanohardness test results.

Analyzing the data given in Table 1 is clear that the rail hardness in as-rolled and workhardened conditions do not have a clear correlation, leading to the conclusion that initial head hardness is almost independent of workhardening ability. This makes the prediction of wear based only on the initial rail's head hardness difficult or invalid. The reason for this is a combination of factors mainly driven by the steel chemistry, heat treatment and thermomechanical processing that have a direct influence in the final microstructural characteristics. For instance, the interlamellar spacing can be closely controlled by conducting the thermomechanical processing at lower temperatures and higher cooling rates. Further, most mechanical properties (including wear) strongly depend on interlamellar spacing. Workhardening was previously reported by Kapoor and Johnson [14,15] when studying the mechanism known as wear by plastic ratcheting. In this theory it is proposed that plastic deformation of the rail occurs due to extrusion of the surface layer. Another wear mechanism taking place on rails is delamination wear [2,14–16].

The depth of the workhardening layer of the rail is a function of the applied load and the mechanical characteristics of the steel. The hardness of the plastic layer decays in a quadratic fashion as a function of depth [30]. The relatively small thickness of the workhardened layer prevents the accurate determination of its hardness, which is attributed to the size of the indenter and indentations of commercial methods (Brinell [31], Rockwell [32] or Vickers [33]). For instance, using microvickers (μHV_{1000}) hardness the size of the indentation for a material with a 500 μHV_{1000} is approximately 60 μm in diameter that falls within the size of the workhardened layer (50–200 μm). Based on the ASTM specification [33] the use of microhardness compromises the accuracy of the results for the workhardened layer. Additionally, Rockwell and Brinell methods do not have the resolution to measure the hardness along the worhardened layer.

Table 1
Results of head hardness analysis conducted on the head of the rails from the "OLD" tests and for the current tests labelled as "Used" (the first two columns of hardness values correspond to the rails tested on the previous test concluded after 435 MGMT (396 MGT) in 2005. The hardness after workhardening corresponds to the measurements taken from the head of the rail at the end of the tests.

Used rail 2001[a]	As-rolled		Workhardened		New rail 2005[a]	Brinell hardness	
	HB	GPa	HB	GPa		HB	GPa
Used 1	399	4.1	461	4.8	D	401	4.4
Used 2	402	4.4	415	4.3	E	430	4.5
Used 3	393	4.1	429	4.5	A	375	3.9
Used 4	390	4.0	415	4.3	C	429	4.5
Used 5	405	4.2	429	4.5	B	415	4.3
Used 6	382	3.8	415	4.3	OLD	395 ± 8.5[b]	4.1

[a] Manufacturing year.
[b] To prevent a direct identification of the rails selected from previous test, the hardness reported in this table for the OLD rail is the average hardness from all rails from previous tests.

Under heavy haul conditions pearlite behaves as a composite-like structure where the Fe-α is soft and ductile, while Fe_3C is the hard component (reinforcement) that acts as an effective barrier for dislocations. Fe-α allows for a relatively easy flow for dislocations allowing plastic deformation. Due to the high stresses (usually above yield strength) the rail is subjected at, Fe-α is plastically deformed and pushed out of the pearlite reaching the surface of the rail and is later removed by the rolling-sliding interaction between the wheels and rails. This creates a starvation of Fe-α near the rail's surface allowing an alignment and concentration of Fe_3C lamellas along the running surface [4,5,7]. This is an effective mechanism that as the traffic increases the workhardened layer develops constantly until it reaches equilibrium stage where the wear rate becomes constant. Thus the wear rate, and workhardening ability, of each rail is different and varies with the chemistry and thermomechanical processing.

Conventional tensile tests conducted using the rails studied in the present work show that steels with higher workhardening ability are those with a narrower difference between yield and tensile strengths. This difference among strengths is a good indicator of wear performance at the beginning of the full scale tests, but does not correlate as well through the entire test. Therefore, it is again difficult to use tensile testing as a way to predict field behaviour, making tribology the ideal testing methodology to determine workhardening ability and rail performance. For this reason the methodology presented in Appendix A was developed as an accurate technique to measure rail workhardening and wear performance.

3.2. Full scale FAST tests

Fig. 4a shows that all test rails exhibited higher wear at the beginning of the tests, compared to the control rail (i.e., the *y*-axis is normalized with the control rail B). However, wear of rails A, C, D and E decreases with accumulated tonnage; for instance rail D shows the highest wear rate (54% more than rail B) at the beginning of the test that was reduced to 7% more than rail B after 229 MGMT (252 MGT). In contrast, rail C at the beginning of the test exhibited 23% higher wear than rail B and after 229 MGMT (252 MGT) this difference was reduced to 4% less than rail B. Therefore, for long term wear, rail C seems to be the best wear performing rail.

Fig. 4b depicts the total wear at FAST, which increases with accumulated tonnage in an almost linear fashion. From Fig. 4b it is evident that for large accumulated tonnages the OLD rail is the worst performing rail, while rails B and C perform better. However, at the beginning of the test, rail B exhibits better wear resistance than rail C but as the traffic accumulates (~175 MGMT) they exhibit comparable wear resistance and after 220 MGMT rail C shows better wear resistance. The disadvantage of this graph is that it is difficult to visualize work hardening effects. In contrast, Fig. 4a shows a clear evolution of the workhardening layer for each rail. Fig. 4a reports the normalized data from the test rails using rail B as the control rail with the aim to enhance work hardening effects; therefore, rail B is equivalent to a ratio = 1. Normalizing wear minimizes the effects, if any, of rail location in FAST and enhances the work hardening ability of each rail.

3.3. Laboratory scale tribology tests

Prior to the use of the ball-on-disk method other tribotest methods were used to validate the technique against other tribotesting methods, including twin disk, nano-scratch and pin-on-disk techniques. The results from these tests could be summarized as follows: nano-scratch testing demonstrated to be effective to identify the workhardening effect showing an exponential decay on wear rate decrease as the number of scratches accumulated. The workhardened layer fully developed after 25–30 scratches [19]. The disadvantage of the nano-scratch technique is the high contact pressure >10 GPa and the small amount of material volume that is analyzed [19]. Ball (Steel)-on-disk and pin-on-disk: similar to the rail-wheel system both components incur wear and the contact pressure progressively decreases during the test. The steel balls and pins were manufactured using wheel steels with hardness close to the ones used in railroad wheels (which is lower than that of the rail). Wear occurred on both the pins/ball and rail, thus difficult to clearly establish rail wear.

In parallel work, the rail workhardening behaviour was successfully analyzed by means of XRD-pole and neutron diffraction; unfortunately this method requires sophisticated equipment and is time consuming [13,18]. Twin disk: there was good correlation between these tests, which better simulate the wheel/rail contact as it includes both sliding and slippage, and the ball-on-disk tests; unfortunately the twin-disk produced extremely small amounts of wear and it required long testing times to have significant measurable wear or RCF [20,21].

In contrast, the adopted ball-on-disk tests had the advantage that exhibit measurable wear volume in a relatively simple way and short time. In addition the ball-on-disk technique has the potential to predict not only workhardening but also rail steel resistance to cracking. Using the ball-on-disk approach with a synthetic ruby ball is possible to conduct tribotesting analysis without incurring any wear on the ruby ball. This allows a direct wear analysis on the rail samples using contact pressures similar to the ones observed in the full scale FAST tests.

3.4. Ball-on-disk wear results

In the present work, an approach to accurately obtain the wear volume was developed and is presented in Appendix A. In this approach the ball-on-disk test considers the total area loss of the wear track (wear volume), and also the total area of the metal flow (shoulders) on each side of the wear track. This approach is similar to the profile overlay method used for the wear data at FAST (Fig. 2). Fig. A1 in Appendix A sketches a wear track taken by the profilometer from the ball-on-disk test showing the three regions that represent the change in area (W_A, W_B, and W_C). The gained area ($W_A + W_C$) is related to the workhardening of the steel and the loss area is related to wear. The sum of the areas W_A, W_B, and W_C are directly related to wear performance. Fig. A1 also shows the four critical points (*a*, *b*, *c*, and *d*) chosen to limit each region. The algorithm used to obtain the wear from such profilometric data is given in Appendix A.

Several approaches are available to compare the results from profile measurements and the ball-on-disk tests. In previous research, the wear analysis of the ball-on-disk measurements was conducted using the depth of the wear track or minimum, indicated as min in Fig. A1. Fig. 5 compares the results of the depths of the wear tracks for the rails manufactured in 2001 and 2005. It is observed that for 600 and 1000 cycles, both generations of pearlitic rail show significantly better wear performance than the bainitic rail, which is attributed to their superior workhardening ability and demonstrating that for rail applications, pearlite is a more desirable microstructure than bainite [1,7]. In addition, Fig. 5 shows that rails manufactured in 2005 (rails A through E) have better wear performance than the rails manufactured in 2001, which is also in direct agreement with the FAST results. The main reason for the better wear performance for the rails manufactured in 2005 is presumably its higher carbon content, but most importantly its finer microstructure [11]. Despite the useful information obtained from such simpler wear analysis, the information is somewhat limited as it does not account for to the pile-up material; in

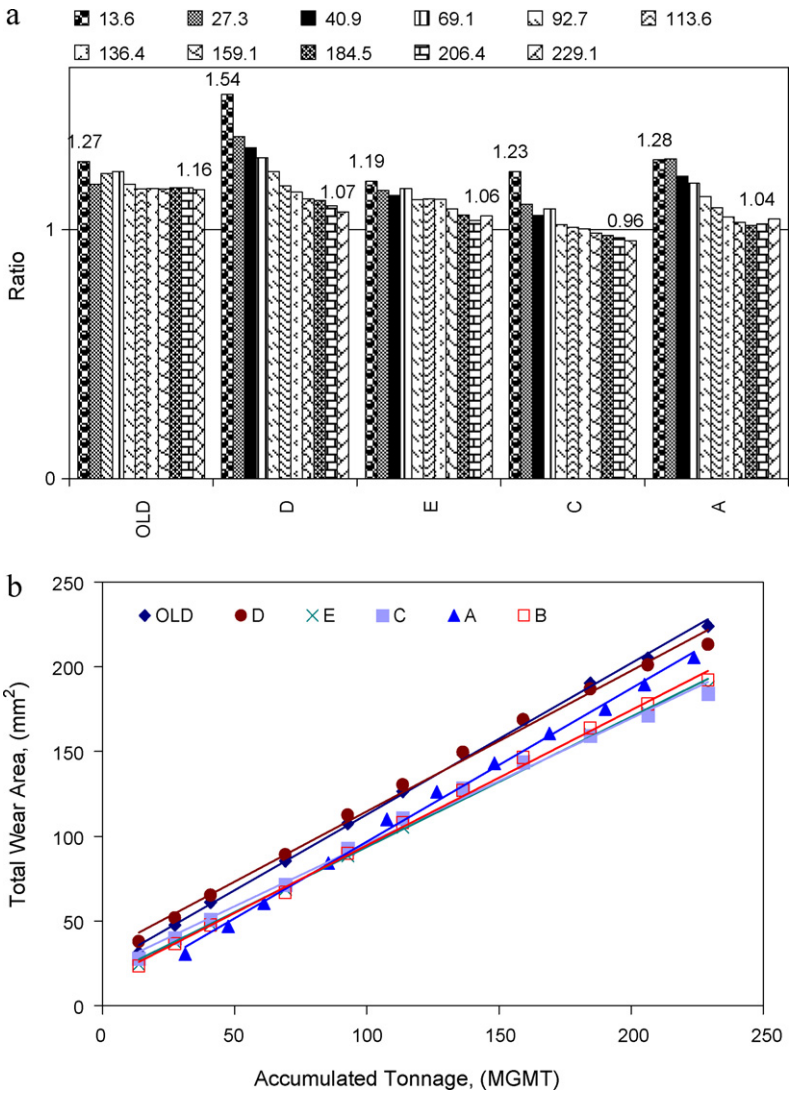

Fig. 4. Workhardening analysis (a) ball-on-disk and (b) full scale FAST tests.

the proposed technique (Appendix A) a detailed analysis has been conducted and is presented in next.

Fig. 6 compares the wear results from the ball-on-disk tests using the approach developed in this work (Appendix A). Fig. 6a shows the amount of material flow along the wear tracks, which is inversely related to the work hardening ability of the tested rails (see Eq. (10) in Appendix A). Fig. 6b presents the wear performance as determined by Eq. (5) in Appendix A for each test. In Fig. 6a, it is observed that rails B, C and E have a rapid response with low material flow and rails OLD, A and D have a slow response with larger material flow. Comparing Fig. 6a and b, the rail OLD shows limited (if any) work hardening, in comparison with the other rails. Rail OLD is the worst performer in the tests completed in 2009, which implies that all rails manufactured in 2005 exhibit better wear performance than the rails manufactured in 2001. Furthermore, this approach also further confirms that that pearlite is a more suitable microstructure than bainite for rail applications, which was confirmed at FAST. Note that bainitic rails exhibit better fatigue resistance compared to pearlitic rails and are more suitable for high impact applications such as rail crossings [22].

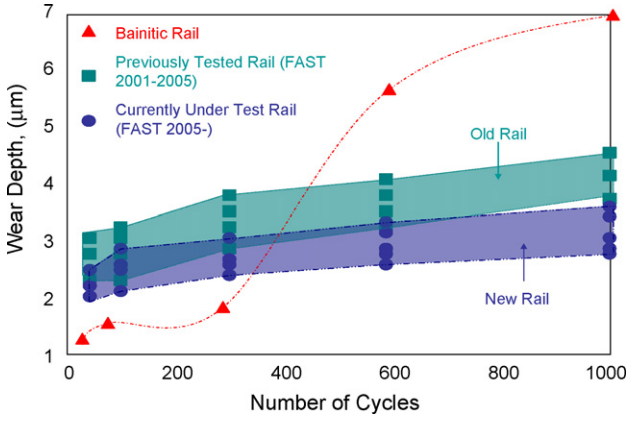

Fig. 5. Analysis of the minimum of the wear tracks from the ball-on-disk tested samples using various premium rails.

As discussed above, effective workhardening has been identified as one of the most desirable properties for premium rails. For this reason, in the ball-on-disk tests, the analysis of the flow of the material (FM) or shoulders is of interest and in this research was found that for each rail the FM is different and these differences are correlated with rail wear performance observed at FAST (see Fig. 4). At the beginning of the ball-on-disk tests the ruby ball has an abrasive effect removing the majority of the steel on its path. The remaining material in the near surface of the track is plasti-

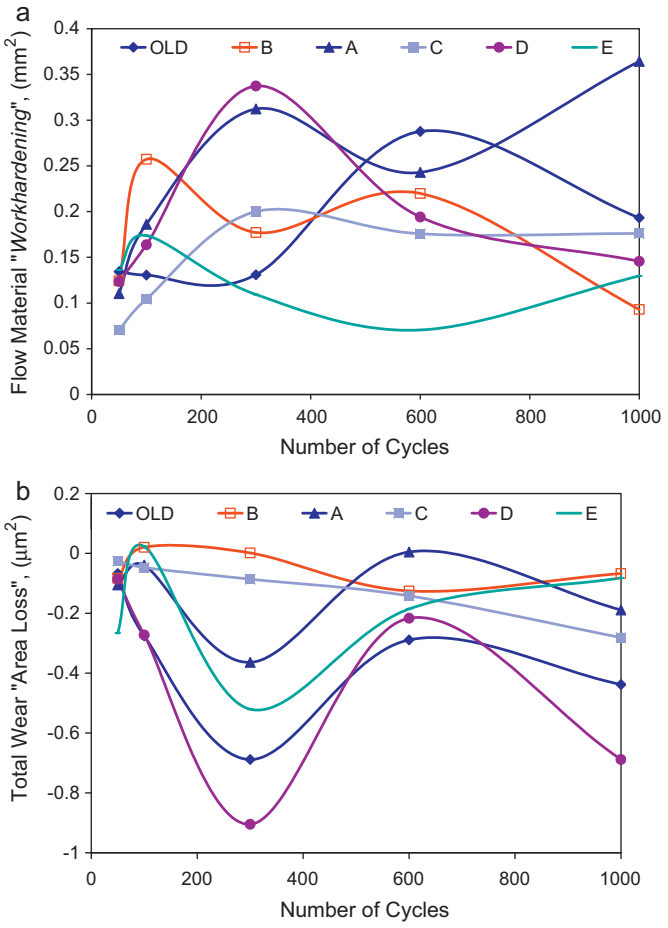

Fig. 6. Ball-on-disk test results for the (a) workhardening analysis and (b) total wear. Notice the opposite performance for low and high cycles.

cally deformed and accumulates (ratcheting) due to cold work. This means that the near surface of the wear track workhardens. The rest of the plastically deformed steel is pushed out of the track forming shoulders (sections A and C in Fig. A1). This effect is repeated during each cycle leaving behind a ratcheting layer that accumulates until this process reaches a steady state and the workhardened layer is completely developed. This in turn is expressed as an increase in hardness and strength due to cold work (dislocation interaction), thus increasing the wear resistance.

A rail with high wear resistance has a rapid workhardening response with low plastic deformation or shoulders along the wear tracks. The analysis of the ball-on-disk data (Fig. 4) shows that small and large shoulders can be related to high and low wear resistant of rails, respectively. In addition, a rail with high wear resistance will start forming the shoulders earlier than a rail with lower wear resistance, which is in agreement with the shakedown phenomena discussed in [34]. This can be interpreted as follows: large shoulders exhibit slow workhardening, allowing continuous removal of the steel that is manifested by the presence of excessive debris. During the ball-on-disk tests, for the lower wear performing rails, a larger portion of the workhardened layer is removed by abrasion and the rest is plastically ploughed delaying the steady state.

Fig. A1 shows two regions, a valley (wear track) and the material flow on each side of the valley. Similar metal flow is observed in the rails at FAST, particularly on the low rail. This "cold working" (extrusion-like) effect was previously explained as a result of plastic ratcheting [13,30]. The wear track represents the total worn metal (Eq. (3)). The material flow (Eq. (10)) corresponds to the plastically deformed steel that is forced out of the wear track forming shoulders. Fig. 4 shows that there is more flow material (sum of areas W_A and W_C) for low wear cycles in sample B than in sample C. However, for high cycles, the opposite behaviour is observed. This indicates that rail B shows a rapid response with a larger amount of FM; however, rail C in the long-term has better workhardening behaviour resulting in higher wear resistance. This finding was further confirmed with the results at FAST, which are depicted in Fig. 4.

4. Wear mechanisms

Rail manufacturers usually heat treat the premium rails to a microstructure mostly composed of fine pearlite (Fig. 7) where the following characteristics can be observed:

(i) Fig. 7a: non-metallic inclusions and pores in the as-polished microstructure
(ii) Fig. 7b: combined ferrite (Fe-α)–cementite (Fe_3C) lamellas typical of pearlite
(iii) Fig. 7c: typical interlamellar microstructure of pearlite
(iv) Fig. 7d: pearlite colony and pro-eutectoid cementite along the prior-austenite grain boundaries and
(v) Fig. 7e: prior austenite grain.

Fig. 7 shows micrographs revealing different constituents of typical microstructures of the ball-on-disk tested rails. The findings from [11,28] indicate that the best wear performing premium rail (manufactured in 2005) posses a prior austenite grain and pearlite colony size approximately 30% smaller with a 12.5% finer interlamellar spacing than the worse wear performing premium rail (manufactured in 2001) [11,28].

Researchers have reported on several wear mechanisms for the wear of steels, including rail steels, such as plastic ratcheting, erosive wear, ploughing and delamination wear [2,15,16,23–25]. In the present work several of these mechanisms were identified for the high performance rails when tested with the ball-on-disk apparatus as well as the rails tested at FAST. In the following section analysis comparing the track surface and debris produced in the ball-on-disk and full scale tests is presented.

Following the ball-on-disk tests, the samples can be distinguished visually between samples with and without or with limited to no debris. Fig. 8a and b depict macrographs of ball-on-disk samples with and without debris in the as-tested conditions for 1000 cycles. The sample without debris (Fig. 8a) is rail B that showed better wear performance, while the sample with debris (Fig. 8b) is rail D, which was a lower performance rail. This may be attributed to a lower wear hardening ability of rail D (Fig. 6). The presence of debris is due to severe wear that removes most of the workhardened layer formed every cycle, delaying the full development of the workhardened layer. Higher strength steel may also produce debris, but of smaller size [26] making its removal during tribotesting easier and this may be the reason why it could not be indentified at the end of the test.

Fig. 8c–f show SEM micrographs of the wear track for the sample presented in Fig. 8a. Specifically Fig. 8c shows a back scattered electron (BSE) image where steel and alumina particles can be seen while Fig. 8d–f shows the effect of the alumina particles. The debris of Fig. 8b shows relatively large amounts of hard inclusions (e.g., alumina). Fig. 8f shows a rough wear surface heavily cracked with plastic deformation and a colony of alumina particles that potentially promote orthogonal cracking. In these figures, the delamination mechanism can be seen (e.g., Fig. 8e) that is initiated by a hard alumina inclusion. Therefore, reducing the amount of alumina in the steel can result in markedly improvements in rail steel performance; recently, it was identified that not only alumina or

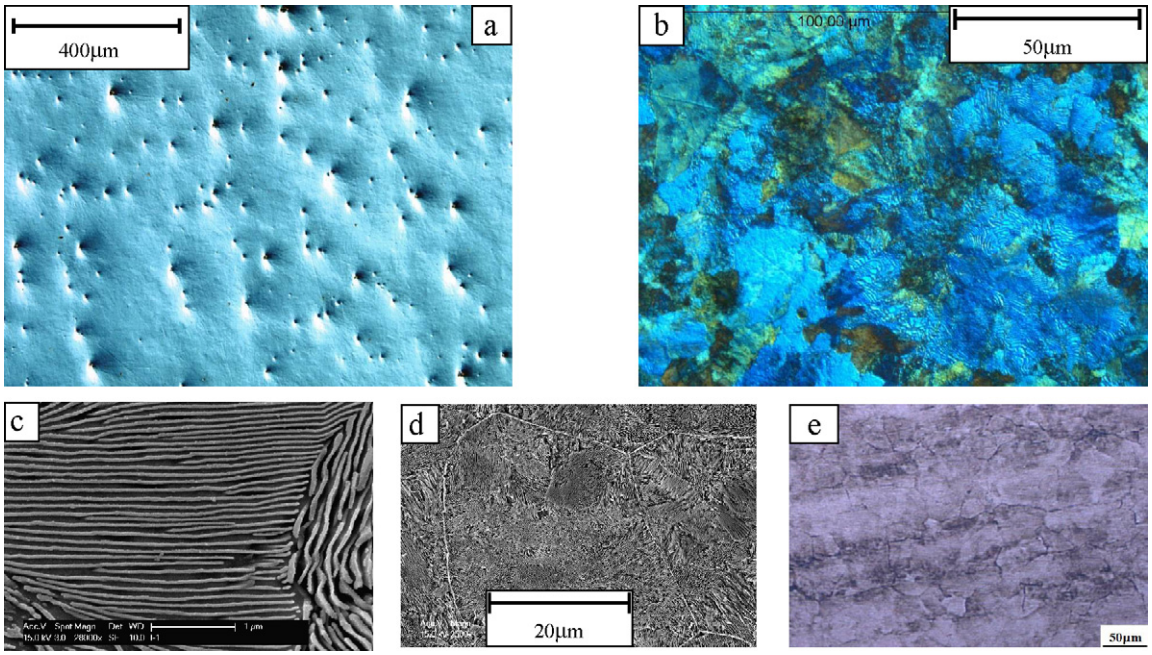

Fig. 7. Characteristic microstructure of premium rails: (a) as polished conditions at 100× and (b) etched at1000×. Examples of the microstructure for randomly selected premium rails showing (c) pearlite interlamellar spacing, (d) pearlite colony size and pro-eutectoid cementite and (e) prior austenite grain.

in general hard inclusions are detrimental for rail steels, but also pro-eutectoid cementite along the prior-austenite grain boundary [11]. At the same time the wear surface besides the delaminated region shows a smooth surface without incurring orthogonal cracking. Fig. 8f shows a family of alumina particles on rail B that created a micro void without promoting orthogonal cracking.

The alumina particle on the right (inset in Fig. 8b) has a negligible contribution to the void formation. The above is an attribute of a good workhardenable steel that results in hardness and strength improvement by preventing crack formation. Workhardening ability can be translated into the material strengthening by preventing dislocation motion (slip or glide). On pearlitic steels, effective workhardening results from its composite-like structure that combines ductile (ferrite) and hard (cementite) constituents. Dislocations slip and/or glide along ferrite. On the contrary, cementite acts as a barrier for dislocations promoting their pile up. For this reason, steels with narrower pearlite interlamellar spacing have a better capacity to prevent dislocation motion and better workhardening ability that makes them more desirable for railroad applications.

Size and distance among hard inclusions seem to also play an important role [27]. Fig. 8f shows the effect of the vicinity of inclusions on steel integrity. The orthogonal cracks presented in Fig. 8f have similar appearance to the cracks developed in the full scale tests or RCF cracks. Potentially, one could attempt to quantify this phenomenon to propose quasi-empirical correlations to extrapolate the orthogonal cracking from ball-on-disk tests to fatigue behaviour of rails in track. Further, the rails showing more RCF at FAST are the rails with higher density of orthogonal cracks during the ball-on-disk tests.

Fig. 9 shows SEM micrographs of two rails with different performance. The samples were tribotested for up to 1000 cycles under identical conditions. The rail with higher performance can be identified by its smoother surfaces (Fig. 9a–c) and the limited plastic deformation at the edges of the wear tracks (i.e., small FM or shoulders). Nonetheless, heavily deformed sections can be observed in Fig. 9c possibly due to dragging effects. Fig. 9b shows the absence of cracks for rail B even at 1000 cycles.

Fig. 9c shows a section with a delaminated region and a hard inclusion that could be the origin of the delaminated layer. During delamination there is crack growth, but the crack grows parallel to the running surface and approaches the surface detaching a thin portion of the hardened layer from the parent rail [23–25]. This mechanism prevents excessive wear thus controlling rail wear due to a slow removal of a near surface layer, which is opposite to the more aggressive mechanism resulting from severe wear and local scuffing.

The lower performance rail is presented in Fig. 9d–f. The SEM micrographs for the sample tested for 300 cycles (Fig. 9d) shows sections with plastic deformation, but in general the surface is relatively smooth. However, the shoulders on this sample are significantly larger than those observed in Fig. 9b. After 1000 cycles, severe wear with local scuffing is observed and the higher magnification images show that this wear mechanism is driven by limited delamination and most of the wear is due to abrasion. Fig. 9 shows the effects of inclusions on the microstructure of tribotested rails. The inclusion shown in Fig. 9e has apparently no effect on the rail material. In the enlarged figure (inset), it is clear that this inclusion was sliced through during the wear process. The chemical makeup of the inclusion is MnS, which is known to be relatively soft. This is opposite to the behaviour observed by the presence of the inclusions presented in Fig. 8f showing limited mechanical damage. In this case, the rail surface presents mechanical damage and a portion of the rail being detached.

Fig. 10 shows optical and scanning electron microscopy images of a spall collected from the low rail at FAST and photographs of rails at FAST. The spall (Fig. 10a) was taken from FAST after approximately 200 MGMT. The spall was cryogenically fractured at the locations indicated by the arrows. In the SEM micrograph shown in Fig. 10b (crack 1) the cold worked structure of the spall shows accumulated ratcheting that results from the heavy haul service environment. It is also observed that crack growth occurs in a transgranular fashion, detaching a layered portion of the rail resulting in delamination. It is of interest to mention that in the cross section of the spall collected from FAST (Fig. 10c and d) there is no evidence of hard inclusions. It is possible that these cracks were initiated inter-

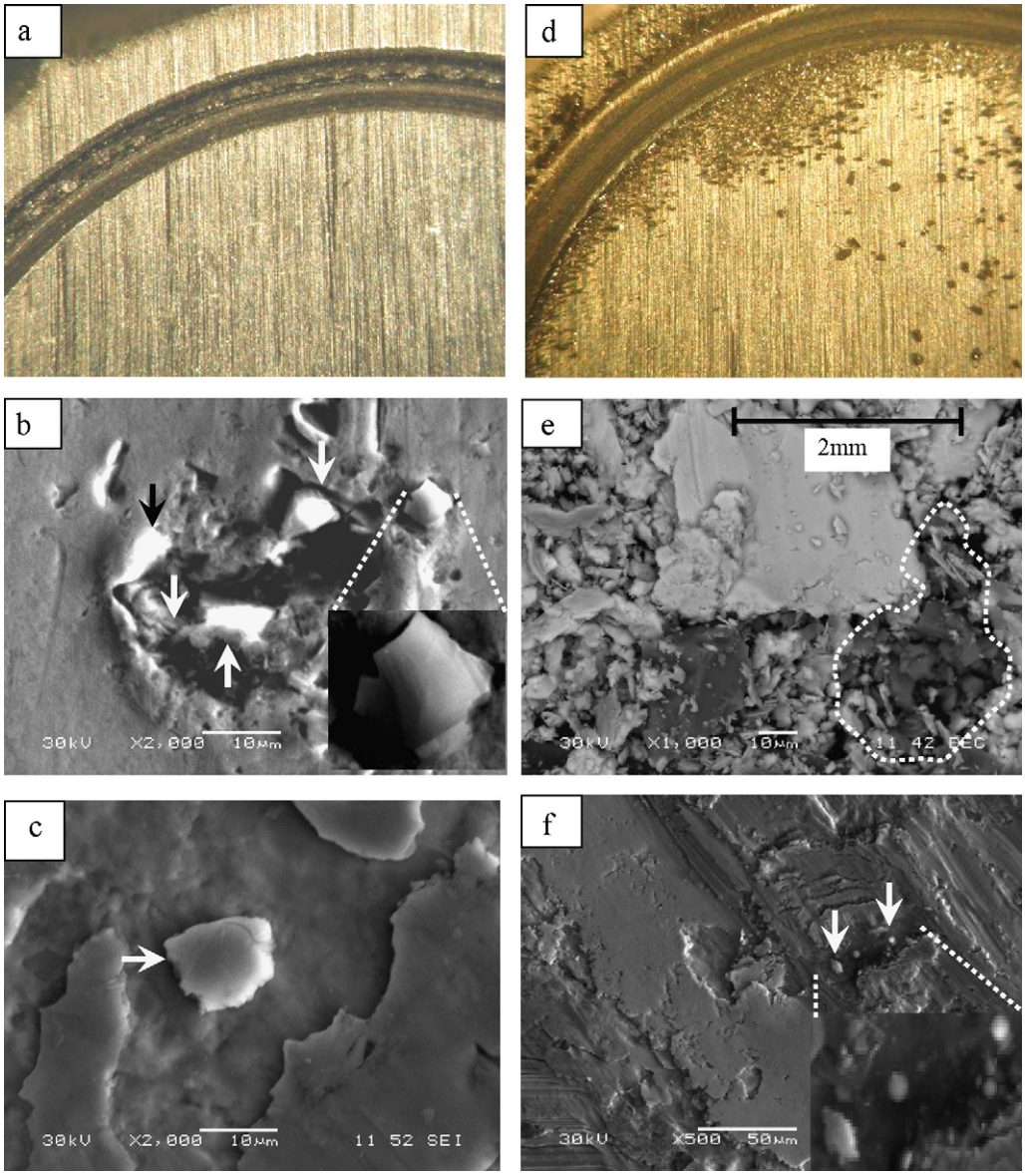

Fig. 8. Ball-on-disk test samples after 1000 cycles showing (a–c) no wear debris (Rail B) and (d–f) wear debris (Rail C). (b–f) Show effect of alumina particles on delamination and crack formation and (e) shows BSE analysis of the debris showing steel and alumina particles. Arrows and dotted lines highlight the alumina particles.

nally and grew transgranularly along the grain boundaries rich in pro-eutectoid cementite [11,28].

Fig. 10c shows SEM micrographs of crack 2 presenting an enlargement of the multilayered nature of the spall due to plastic deformation and Fig. 10d shows the respective EDX analysis (Pd in the EDX spectrum is from the coating used for sample preparation). Fig. 10f and g present two images of two rails currently under test at FAST with the same accumulated tonnage; one shows a shinny surface and the other shows a heavily cracked surface. Both rails were located in the low rail and from these pictures we can compare the difference in RCF performance. The orthogonal cracks were enhanced using dye penetrants and are identified in the gage side of the rail. In the field side of the rail we can be observed the FM or shoulders. The FM is also presented in Fig. 10g for rails removed from revenue service at the end of the previous test (rail manufactured in 2001) clearly showing the difference in wear and the corresponding shoulder. Fig. 10 is evidence that some of the wear mechanisms observed in the full scale test can be investigated at the laboratory level using a ball-on-disk test.

5. Workhardeing mechanisms

The pearlite and workhardening phenomenon of premium rails is complex and in some cases the constituents at the prior-austenite grain (pro-eutectoid cementite, precipitates, etc.) are playing a significant role (Fig. 7b). It is well known that rail steels with narrower pearlite have better mechanical properties. This is because by refining pearlite, the number of barriers for dislocations increases resulting in a faster development of the workhardened layer. Coarser pearlite limits the number of barriers for dislocations allowing faster dislocations and micro crack initiation.

Interlamellar spacing on pearlite is considered the most influential parameter of the microstructure to mechanical properties (e.g., hardness and strength) on pearlitic steels. It is expected that finer microstructures show better rail performance. Interlamellar spacing is a function of alloying elements (e.g., carbon) and thermomechanical processing. The carbon content of rails manufactured in 2005 is up to 0.3 wt% C higher than the high strength or standard strength metallurgies with additions of other elements. The higher

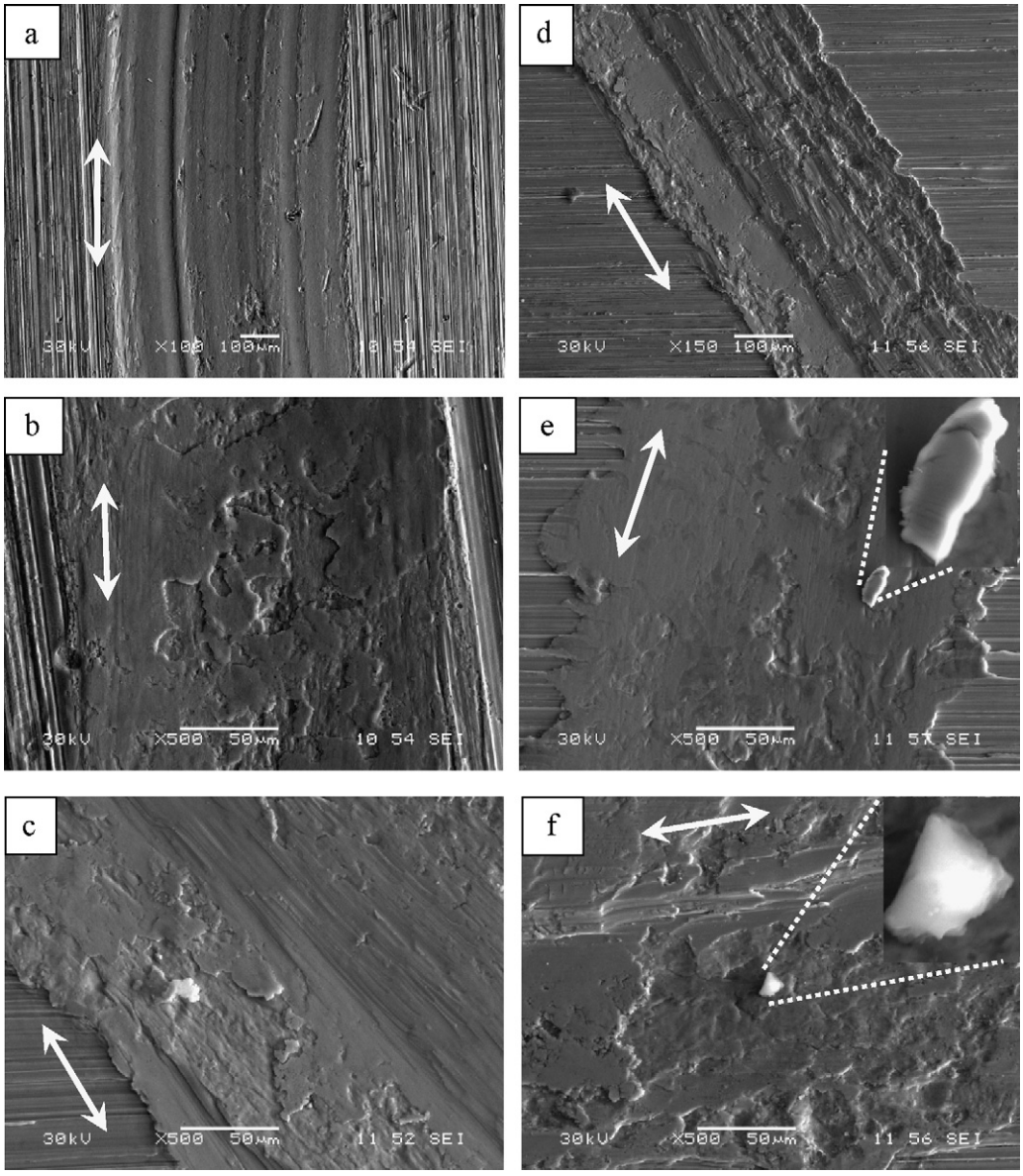

Fig. 9. SEM micrographs of the wear tracks of ball-on-disk samples from two rails after tribotesting for (a–c) higher and (d–f) lower wear performance rails. Samples tested for 300 (a and b) and 1000 (c and f) cycles. Note the highly deformed edges (track shoulders) on the lower wear performing rails. Arrows indicate the sliding direction.

carbon content together with the other alloying elements present in the rails manufactured in 2005 have finer microstructure, resulting in better performing rails. For example, the interlamellar spacing of the premium rails investigated in this work is between 50 nm and 400 nm, which are finer than older generation rails. This refinement resulted in an increase in hardness from 100 HB to 240 HB [11,28,35,36]. Unfortunately, there are no experimental results in the literature to that perform a direct comparison among rail performance improvements between the older rail steel generations and the premium rails investigated herein. However, by looking at the differences in microstructure and hardness, it can be concluded that premium rails have superior wear performance over rails previously developed and reported in the literature.

The differences in wear performance for the tested rails are related to the microstructure and hence the mechanical properties of rails. Taleff et al. [26] developed a methodology to estimate mechanical properties of steels as a function of their microstructure. In such methodology, for pearlitic steels is considered interlamellar spacing, prior austenitic grain and pearlite colony size. Another method includes the strengthening mechanism described by Hall-Petch, where grain boundaries are considered effective strengtheners. Current findings [11,28] indicate that the best wear performing premium rail (manufactured in 2005) possess a prior austenite grain and pearlite colony size approximately 30% smaller with a 12.5% finer interlamellar spacing than the worse wear performing premium rail (manufactured in 2001) [11,28].

The workhardening mechanism can be explained as the accumulation of plastic deformation (e.g., dislocations) that builds residual stresses near the surface of the rail. This is an accumulative phenomenon that increases with traffic and is expected that the ideal rail steel is one that has the ability to develop the workhardened layer more rapidly. In the opposite case, generated shoulders on both sides of the wear tracks are continuously growing because the applied load is always above the shakedown limits of the material. This allows abrasion and easy removal of the steel along the ruby ball path delaying the formation of the workhardened layer. Similar mechanisms for the workhardening phenomena are observed in both ball-on-disk and full scale tests, demonstrating

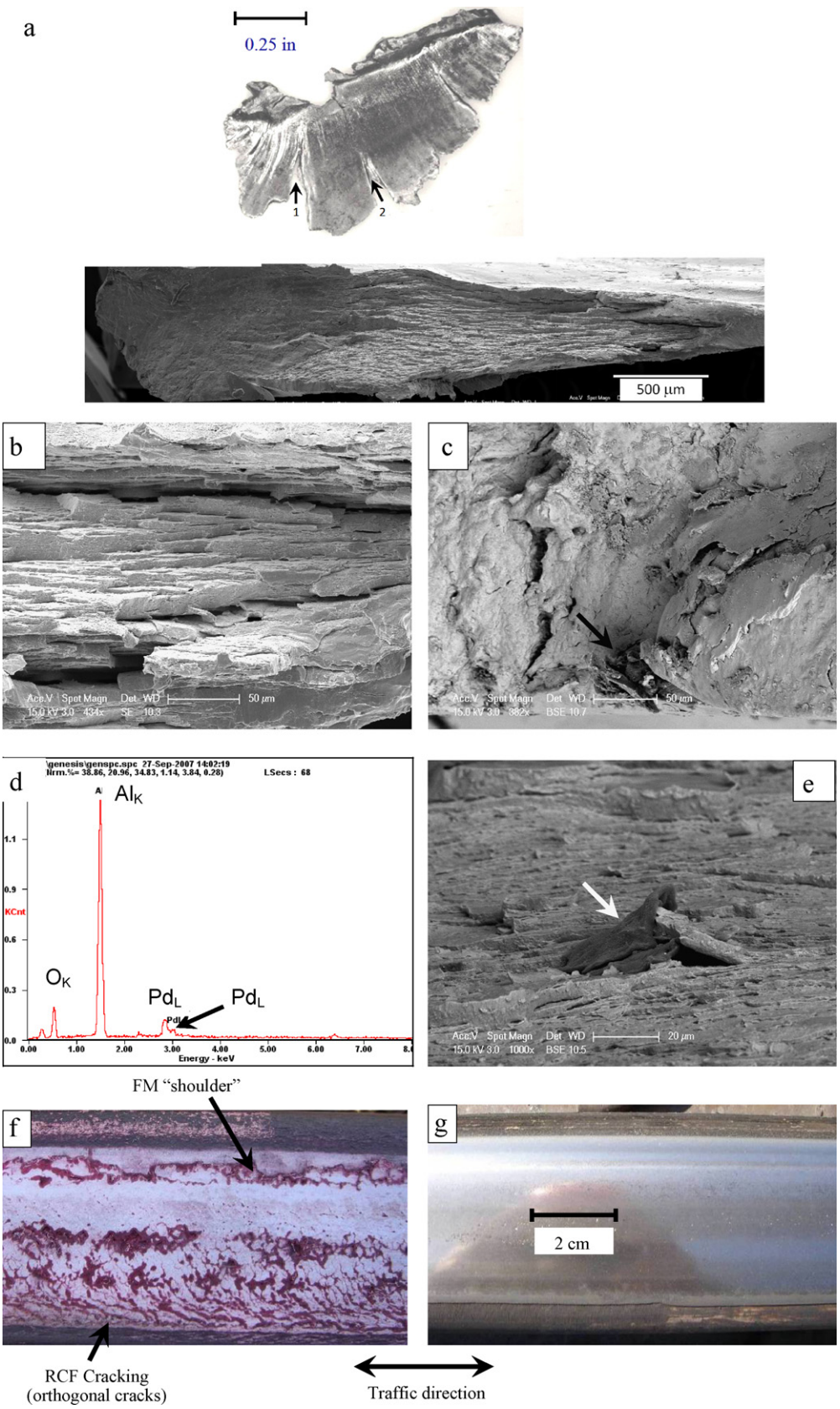

Fig. 10. (a, f and g) Optical and (b–e) SEM analysis of the rails showing the analysis of a spall (a–f) taken from Rail C collected at FAST (rail with relatively large amount of inclusions). (b) Shows accumulated ratcheting observed along the cross section of the spall, the effect of (c) hard (alumina) and (e) soft (MnS) inclusions on rail steels, (g) rail with rough surface due to RCF and (f) rail showing a smooth surface (no RCF). Notice that both rails were subjected to the same amount of traffic and were tested at the same time.

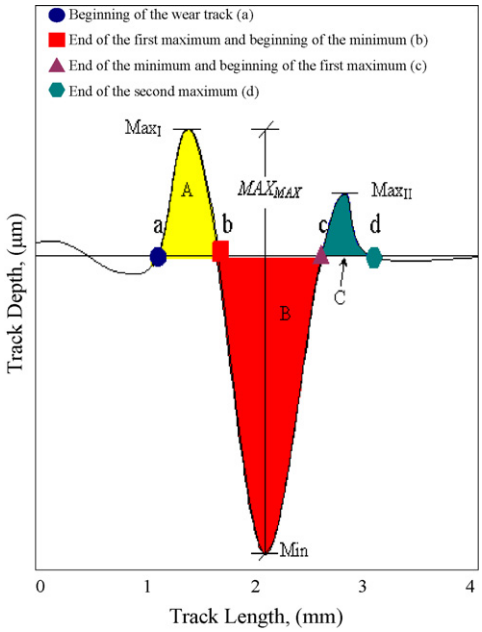

Fig. A1. Sketch of a typical wear profile measured using contact profilometry along the wear track from a ball-on-disk sample showing the main points used for the algorithm developed in this research.

that the ball-on-disk test is suitable to predict rail performance.

Wear and fatigue resistance are driven by different mechanisms which are almost independent. Wear is mainly a function of microstructure and workhardening ability of the steel. On the other hand, the cracking propensity is an intrinsic phenomenon that depends on the grain boundaries nature and the presence of inclusions (mainly hard inclusions) along with the shakedown limits of the steel [27]. Since all rails are different in composition and thermomechanical manufacturing, it is expected that all of them have different wear performance; nonetheless, their performance is a direct function of the above mentioned characteristics. It can be said that the less desirable wear condition is when severe delamination and abrasion act together. Particularly, when severe abrasion occurs it results in excessive cracking developing undesirable wear mechanisms such as scuffing.

Comparing the effects of the inclusions presented in Figs. 8c and 9e against the inclusions in Figs. 8f and 9f the different effects of soft and hard inclusion can be observed that confirm that the nature (soft or hard) of the inclusion itself play an important role. This effect observed in the tribo-test is further confirmed in the FAST tested rails in Fig. 10c and e. Hard inclusions are in general more detrimental for the integrity of the rails. It is not the intention to say that MnS inclusions have no effect on rail performance, but rather that soft inclusions are less detrimental to wear.

6. Conclusions

Based on detailed comparison and analysis of laboratory ball-on-disk experiments using actual rail samples and full-scale rail experiments, it can be concluded that using the simple ball-on-disk test method and an algorithm to accurately calculate wear and material flow, it is possible to directly assess rail performance. For instance, wear performance has a good correlation among flow material and workhardening behaviour. In addition, analyzing the wear track under SEM is possible to identify different wear behaviours that can be used to determine rail crack propensity under pure sliding conditions. The analysis presented and discussed in this work leads to the conclusion that there is a good correlation among the ball-on-disk and FAST tests. This in turn, confirms the potential of the ball-on-disk test method not only to investigate wear performance but also rail crack tendency and to predict rail performance at the laboratory level. A limitation of this method is that it is not qualitative and at this point it is not possible to assess the life time spam for rails using this method. Nonetheless, the ball-on-disk method is a reliable tool and can be used as a pre-screening rail performance method.

Workhardening ability and crack propensity are characteristics that can be determined using the ball-on-disk method. In previous approaches there were necessary at least three testing methods (pin-on-disk, twin disk and nano-scratch) to accomplish the determination of these characteristics [13–21]. In the present work it is demonstrated that a single method (ball-on-disk) is capable of investigating workhardening and crack propensity characteristics and has the advantage that it is a simpler methodology and requires less effort and time. More importantly, the ball-on-disk results are in agreement with the FAST results.

Acknowledgments

Results conducted in this work were partially funded by Federal Railroad Administration (FRA) and the Association of American Railroads (AAR). The UIUC would like to thank the U.S.-DOE for the grant DEFG02-91-ER45439 that support the centre for microscopy. FCRH wants to give special thanks to Dr. K. Hou from TTCI for his diligent and highly educated discussions to understand the contact fatigue phenomena of premium rails. FCRH appreciates the funds from the Government of Texas, TTCI and the University of Houston for the HEAFS, 00730/5022/H0139/B0100/G097746 and Start-up funds respectively.

Appendix A. Algorithm for wear analysis from ball-on-disk tests

The following methodology was developed as a standard procedure used in Matlab and OriginLab software to automatically evaluate the results of the contact profilometer and to make it a standard method for a more accurate and rapid analysis. Eq. (1) expresses the total area of the wear track.

$$W_T = \int_a^d W dx - \int_a^d W_{zero} = \Delta W\big|_{[0<x<4]} \quad (1)$$

where W_T represents the total wear, dx indicates the location across the wear track from 0 to 4 mm (0 to 0.16 in.), W_{zero} represents the zero curve or baseline (BL), that in this particular case is equal to zero. ΔW represents the volume change along the wear track and $[0<x<4]$ limits for the profile was measured along the "x" direction.

The wear volume of the individual areas shown in Fig. A1 can be determined as (W_A, W_B, and W_C) as follows in Eqs. (2)–(4):

$$W_A = \int_a^b W dx = \sum_a^b W\Delta x \quad (2)$$

$$W_B = \int_b^c W dx = \sum_b^c W\Delta x \quad (3)$$

$$W_C = \int_c^d W dx = \sum_c^d W\Delta x \quad (4)$$

Since $W_{zero} = 0$; W_A and W_C are positive and W_B is negative. Therefore, the total wear is expressed as a function of their indi-

vidual integrals or additions as shown in Eq. (5):

$$W_T = \int_a^b W dx + \int_b^c W dx + \int_c^d W dx \quad \text{or} \quad W_T = \sum_a^b W\Delta x + \sum_b^c W\Delta x + \sum_c^d W\Delta x \tag{5}$$

To determine the values of the maxima and minima, the first derivative must be determined as the limit approaches zero, Eqs. (6)–(8).

$$\max_I = \lim_{\delta x \to 0} \frac{a(W_A + X) - a(W_A)}{X} \quad \text{or} \quad \lim_{\delta x \to 0} \frac{dW_A}{dx} \tag{6}$$

$$\min = \lim_{\delta x \to 0} \frac{b(W_B + X) - b(W_B)}{X} \quad \text{or} \quad \lim_{\delta x \to 0} \frac{dW_B}{dx} \tag{7}$$

$$\max_{II} = \lim_{\delta x \to 0} \frac{c(W_C + X) - c(W_C)}{X} \quad \text{or} \quad \lim_{\delta x \to 0} \frac{dW_C}{dx} \tag{8}$$

Usually one of the two maxima is larger than the other one and is identified as $\max_{max}$. The approach followed for the wear performance analysis in Fig. A1 can be expressed using Eq. (9):

$$H = \max_{max} + \left|\min\right| \tag{9}$$

Analyzing individual wear volumes (W_A, W_B, and W_C) using Eqs. (2)–(4) did not lead to a conclusive determination of the wear performance for individual rails. For this reason the sum of the volumes W_A, W, and W_C was obtained and is comparable to the analysis performed using MiniProf. Eq. (9) was used in previous research to represent wear performance and was a simple and reasonable approach to determine the effect of rail microstructure and distinguish between the two generations of rail [10]. A more complete analysis can be conducted by determining the full integral (Eqs. (1)–(5)) leading to a clear identification of the wear performance for each rail that matches with the full-scale test results from FAST.

The analysis of the flow (Eq. (10)) is an indirect approach that in this particular work was used to identify workhardening.

$$FM = W_A + W_C = \int_a^b W dx + \int_c^d W dx \quad \text{or} \quad \sum_a^b W\Delta x + \sum_c^d W\Delta x \tag{10}$$

This analysis approach using the ball-on-disk test considers the total area loss of the wear track (wear volume), and also the total area of the metal flow (shoulders) on each side of the wear track. This approach is much like the profile overlay method used for the data at FAST. The sum of the areas W_A, W_B, and W_C is directly related to wear performance. Approaches have been proposed to compare the results from profile measurements and the ball-on-disk tests with FAST results. For instance, in earlier research, the wear analysis of the ball-on-disk measurement was conducted using the depth of the wear track or minimum, indicated as min in Fig. A1 [1]. Unfortunately this approach has limited accuracy as shown in Fig. 5.

References

[1] F.C. Robles Hernández, N.G. Demas, D.D. Davis, A.A. Polycarpou, L. Maal, Mechanical properties and wear performance of premium rail steels, Wear 263 (1–6) (2007) 766–772.
[2] N.P. Suh, The delamination theory, Wear 25 (1973) 111–124.
[3] J. Kristan, K. Sawley, D. Canadinc, K.M. Lee, A.A. Polycarpou, H. Sehitoglu, Wear and rolling contact fatigue in bainitic steel microstructures, in: 6th International Conference. Contact Mech. and Wear of Rail/Wheel Systems, Gothenburg, Sweden, 2003.
[4] P. Clayton, K.J. Sawley, P.J. Bolton, G.M. Pell, Wear behavior of bainitic steels, Wear 120 (1987) 199–220.
[5] N. Jin, P. Clayton, Effect of microstructure on rolling/sliding wear of low carbon bainitic steels, Wear 202 (1997) 202–207.
[6] J. Kristan, Preliminary Results of AAR Developed 'J6' Bainitic Rail Tested in Revenue Service, Association of American Railroads, Transportation Technology Center, Inc. Research Report No. RR-02-011, Pueblo, Colorado, 2002.
[7] K.M. Lee, A.A. Polycarpou, Wear of conventional pearlitic and improved bainitic rail steels, Wear 259 (2005) 391–399.
[8] K. Sawley, R. Jimenez, The Comparative Wear Performance of Premium and Bainitic Rail Steels under Heavy Axle Loads, AAR Report No. R-941, Association of American Railroads, Transportation Technology Center, Inc., Pueblo, Colorado, 2000.
[9] K. Sawley, J. Kristan, Development of bainitic rail steels with potential resistance to rolling contact fatigue, Fatigue & Fracture of Engineering Materials & Structurees No. 26, Sheffield, UK, 2003, 1019–1029.
[10] F.C. Robles Hernandez, Advanced Rail Steels 4A FAST Rail Performance, Association of American Railroads, HALRC-ERC 2005 Fall Meeting, HALRC/ERC Fall 2005, Pueblo, Colorado, 2006.
[11] R. Ordóñez Olivares, C.I. Garcia, A. DeArdo, S. Kalay, F. C. Robles Hernández, Advanced Metallurgical Alloy Design and Thermomechanical Processing for Rails Steels for North American Heavy Haul Use, Wear, doi:10.1016/j.wear.2010.10.048, in press.
[12] Chapter 4, American Railway Engineering and Maintenance-of-the-Way Association (AREMA), Rail Specifications 4-2-1, 2006.
[13] D. Canadinc, K.M. Lee, H. Sehitoglu, A. A. Polycarpou, Linking microstructure–mechanical properties–wear performance, Final Report submitted by the University of Illinois, Urbana-Champaign to TTCI, May 18, 2006.
[14] A. Kapoor, K.L. Johnson, Plastic ratcheting as a mechanism of erosive wear, Wear 186–187 (1995) 86–91.
[15] A. Kapoor, Wear by plastic ratcheting, Wear 212 (1997) 119–130.
[16] S. Jahamnir, N.P. Suh, E.P. Abrahamson, Microscopic observation of the wear sheet formation by delamnation, Wear 28 (1974) 235–249.
[17] Y.N. Taran, V.I. Novik, Microhardness of cementite, Mater. Sci. Heat Treat. 13 (1971) 818–820.
[18] D. Canadinc, H. Sehitoglu, H.J. Maier, P. Kurath, On the incorporation of length scales associated with pearlitic and bainitic microstructures into a visco-plastic self-consistent model, Mater. Sci. Eng.: A 485 (2008) 258–271.
[19] K.M. Lee, A.A. Polycarpou, Micro/nano scale wear behavior of pearlitic and bainitic rail steels, in: Proceedings of the World Tribology Congress III – 2005, 2005, pp. 795–796.
[20] F. Alwahdi, F. Franklin, A. Kapoor, Primary Testing of Normal Head-Hardened and J6 Bainitic Rail Ssteels, University of Sheffield, 2003, p. 25.
[21] G. Vasic, F.J. Franklin, A. Kapoor, Wear Testing of Deep Head-Hardened (DHH), Normal Head-Hardened (Nippon) and Bainitic (J6) Rail Steels, The University of Newcastle upon Tyne, 2004, p. 37.
[22] P. Clayton, D. Danks, Effect of interlamellar spacing on the wear resistance of eutectoid steels under rolling-sliding conditions, Wear 135 (1990) 369–389.
[23] N.P. Suh, An overview of the delamination theory of wear, Wear 44 (1977) 1–16.
[24] N.P. Suh, N. Saka, S. Jahanmir, Implications of the delamination theory on wear minimization, Wear 44 (1977) 127–134.
[25] F.C. Robles Hernandez, J. LoPresti, D. Davis, A. Polycarpou, H. Sehitoglu, Mechanical properties and wear performance of premium rail steels, in: 86th TRB Meeting, Washington, DC, 2007, pp. 21–25.
[26] E.M. Taleff, C.K. Syn, Pearlite in ultrahigh carbon steels: heat treatment and mechanical properties, Metall. Mater. Trans. A (1995).
[27] T. Murikami, M. Endo, Effects of defects, inclusions and inhomogeneities on fatigue strength, Fatigue 16 (1994) 163–182.
[28] F.C. Robles Hernandez, S. Kalay, R. Ordoñez Olivares, C. Isaac Garcia, A. DeArdo, Development of the new rail steels for the 21st century, in: 8th International Conference on Contact Mechanics and Wear of Rail/Wheel Systems (CM2009), Firenze, Italy, September 15–18, 2009.
[29] F.C. Robles Hernández, R. Ordóñez Olivares, D. Szablewski, C.I. Garcia, A. DeArdo, S. Kalay, Development of the next generation rail steels for heavy axle loads, in: International Heavy Haul Conference, Shangai, China, June 22, 2009.
[30] A. Kapoor, J.A. Williams, Shakedown limits in sliding contacts on a surface-hardened half-space, Wear 172 (2) (1994) 197–206.
[31] ASTM standard E 10–10-07a, Standard test methods for brinell hardness of metallic materials, 3.01, 2007, 123–154.
[32] ASTM standard E 18–10-07a, Standard test methods for Rockwell hardness of metallic materials, 3.01, 2007, pp. 123–154.
[33] ASTM standard E 92–82, Standard test method for Vicker hardness of metallic materials, 3.01, 2007, pp. 123–154.
[34] A.F. Bower, K.L. Johnson, Plastic flow and shakedown of rail surface in repeated wheel-rail contact, Wear 144 (1991) 1–18.
[35] M.G. Mendes da Fonseca Gomes, L.E. Almeida, L.C.F.C. Gomes, I.L. May, Effects of microstructural parameters on mechanical properties of eutectoid rail steels, Mater. Charact. 39 (1997) 1–14.
[36] D.E. Parson, D.A. Munro, J. Ng-Yelim, Vanadium/nitrogen modification of 1% Cr and Cr–Cb rail steels, Can. Metall. Q. 22 (4) (1983) 475–483.
[37] J.H. Beynon, J.E. Garnham, K.J. Sawley, Rolling contact fatigue of three pearlitic rail steels, Wear 192 (1–2 (March)) (1996) 94–111.
[38] J.H. Beynon, J.E. Garnham, K.J. Sawley, Rolling contact fatigue of three pearlitic rail steels, Wear 192 (1996) 94–111.
[39] P. Clayton, K.J. Sawley, P.J. Bolton, G.M. Pell, Wear behavior of bainitic steels, Wear 120 (2) (1987) 199–220.